Stem Cell Reviews and Reports
https://doi.org/10.1007/s12015-022-10503-z

EGFL7 Secreted By Human Bone Mesenchymal Stem Cells Promotes Osteoblast Differentiation Partly Via Downregulation Of Notch1-Hes1 Signaling Pathway

Weijun Zhang[1,2,3,4] · Jinwu Bai[1,2,3,4] · Lijun Li[1,2,3,4] · Ye Zhang[1,2,3,4] · Kai Hang[1,2,3,4] · Yibo Wang[1,2,3,4] · Zhongxiang Wang[1,2,3,4] · Chenyi Ye[1,2,3,4] · Deting Xue[1,2,3,4]

Accepted: 23 December 2022

Abstract

Background Epidermal growth factor-like domain protein 7 (EGFL7) is a secreted protein that is differentially expressed in the bone microenvironment; however, the effect of EGFL7 on the osteogenesis of human bone marrow mesenchymal stem cells (hBMSCs) is largely unknown.

Methods EGFL7 expression in the fracture microenvironment was analyzed based on the Gene Expression Omnibus (GEO) database. Knockdown of EGFL7 by small interfering RNA (siRNA) and in vitro stimulation with recombinant human EGFL7 (rhEGFL7) protein were used to assess alterations in downstream signaling and changes in the osteogenic differentiation and proliferation of hBMSCs. A γ-secretase inhibitor was used to further explore whether inhibition of Notch signaling rescued the osteogenic-inhibitory effect of EGFL7 knockdown in hBMSCs. A femoral defect model was established to verify the effect of recombinant mouse EGFL7 on bone healing in vivo.

Results EGFL7 expression increased during hBMSC osteogenesis. Knockdown of EGFL7 impaired hBMSC osteogenesis and activated Notch1/NICD/Hes1 signaling. rhEGFL7 promoted hBMSC osteogenesis and downregulated Notch1 signaling. The osteoblast-inhibitory effect of EGFL7 knockdown was rescued by Notch1 signaling inhibition. Recombinant EGFL7 led to enhanced bone healing in mice with femoral defects.

Conclusions EGFL7 promotes osteogenesis of hBMSCs partly via downregulation of Notch1 signaling.

Keywords $EGFL7_1$ · $Notch_2$ · Hes_3 · $hBMSCs_4$ · $Osteogenesis_5$

Introduction

Non-healing fractures remain an important clinical problem, with high costs to individuals and society in terms of pain, financial burden, and loss of employment [1]. In the United States, approximately 600,000 fractures each year result in delayed union; nearly 100,000 progress to nonunion. According to a study of 853 patients, the average treatment cost for patients with tibial fracture nonunion was $25,555.97, almost twice as much as for patients with normal healing ($11,686.24). Patients with nonunion are also more likely to use potent opioids than those without nonunion, and for nearly twice the length of time [2]. Understanding the fracture microenvironment can provide additional insights into the mechanisms of bone healing. The fracture microenvironment is enriched with cytokines and growth factors that contribute to the repair of bone and soft tissue [3]. Exploring the specific roles of these factors

Weijun Zhang, Jinwu Bai, Lijun Li these authors contributed equally to this article.

✉ Deting Xue
blueskine@zju.edu.cn

1 Department of Orthopedic Surgery, the Second Affiliated Hospital, Zhejiang University School of Medicine, Zhejiang Province, Hangzhou City, People's Republic of China

2 Orthopedics Research Institute of Zhejiang University, Zhejiang Province, Hangzhou City, People's Republic of China

3 Key Laboratory of Motor System Disease Research and Precision Therapy of Zhejiang Province, Zhejiang Province, Hangzhou City, People's Republic of China

4 Clinical Research Center of Motor System Disease of Zhejiang Province, Hangzhou City, People's Republic of China

Published online: 07 January 2023

has important implications for strategies to accelerate bone healing.

Epidermal growth factor-like domain protein 7 (EGFL7; also known as VE-stain, Zneu1, Neu1, Notch4-like, and Tango125) has recently been found to be expressed in growth plate cartilage [4, 5] and to regulate stem cell fate [6]. EGFL7 cDNA was first cloned by Soncin et al. (2003), when he named it vascular endothelial statin (VE-stain) [7]. EGFL7 consists of an Emilin-like structural domain (EMI) and two EGF-repeats. The EGFL7 gene is present on chromosome 9 (9q34.3) and 2 in humans and mice, respectively [7]. EGFL7 has been shown to be downregulated in almost all mature tissues [8] and strongly upregulated in proliferating tissues (e.g., tumors, gestational reproductive organs, and inflamed tissues) [9]. EGFL7, with a relative molecular weight of 29 kDa and 278 amino acids, can be deposited in the extracellular matrix (ECM) with a head-to-tail linkage. EGFL7, widely recognized as a potential cancer therapeutic target [10], causes a circulating T cell deficiency (Flt3 signaling pathway) [11], inhibits T cell recruitment (ICAM and VCAM on ECs) [12], and downregulates ECM stiffness (LOXL2) [13, 14]. EGFL7 has been reported to control the proliferation or migration of malignant brain tumors [15, 16], clear cell renal cell carcinoma [17], and acute myeloid leukemia (AML) [18]. However, the role of EGFL7 in the osteogenic differentiation of human bone marrow mesenchymal stem cells (hBMSCs) is unknown. In this study, we examined the effects of EGFL7 on the osteogenesis of hBMSCs. Our results demonstrate that EGFL7 promotes the osteogenesis of hBMSCs in vitro and in vivo.

Materials and Methods

Differential Expression Analysis

The dataset was downloaded from the GEO database (http://www.ncbi.nlm.nih.gov/geo). Three 2-month-old and three 24-month-old fracture samples were included in the GSE166441 dataset [19]. The limma package was used to determine differentially expressed genes (DEGs) [20]. The normalized mRNA expression profiles were downloaded directly, and genes meeting the criteria of a fold change > 1.5 and $p < 0.05$ were considered significantly different. In total, 1296 DEGs were identified. The Ggplot2 package was used to draw volcano plots showing EGFL7 expression patterns in 24- and 12-month fracture samples.

Protein–Protein Interaction (PPI) Network Construction

A PPI network for EGFL7 was constructed using the STRING [21] (http://string-db.org) and GeneMANIA [22] (https://genemania.org/) databases. Thirty-eight EGFL7-related genes were screened in STRING using the protein interaction screening medium criteria (confidence, $n = 0.4$) as a threshold. GeneMANIA identified 20 genes with strong correlation to EGFL7. The size of the circle indicates the correlation, and the color indicates the Gene Ontology (GO) annotation function of each of the different functional modules.

GO and Pathway Enrichment Analyses

The clusterProfiler package [23, 24] was obtained from Bioconductor (http://bioconductor.org/). GO enrichment analysis [25] was performed on 38 EGFL7-related genes obtained from the STRING database. A bubble chart of biological function annotation was drawn using the ggplot2.dotplot() function; $p < 0.05$ values were considered statistically significant. WikiPathways in Enrichr [26, 27] (https://maayanlab.cloud/Enrichr) was used for pathways analysis and the results were ranked according to their combined scores.

Cell Culture and Reagents

hBMSCs were purchased from Cyagen Biosciences (Guangzhou, China; HUXMA-01001) and cultured in adult bone marrow mesenchymal stem cell complete medium (Cyagen Biosciences; HUXMA-90011). At 37 °C in a 5% CO_2 incubator, hBMSCs were adhered in Corning® 25 cm^2 culture flasks (Corning, NY, USA; 3289) and subjected to 1:3 passaging with Cienry® trypsin (Zhejiang, China; CR-25200) when grown to 90% confluence. Second to eighth generation cells were used for additional experiments. Exogenous recombinant human and mouse EGFL7 (rhEGFL7 and rmEGFL7, respectively) were purchased from Sino Biological (Beijing, China; 11,979-H07B and 50,472-M07B). Three small interfering RNAs (siRNAs) and overexpression lentivirus targeting the EGFL7 gene were designed by GenePharma (Shanghai, China): EGFL7-Homo-187 sense (CACCUACCGAAC CAUCUAUTT), EGFL7-Homo-187 antisense (AUA GAUGGUUCGGUAGGUGTT), EGFL7-Homo-400 sense (CCAGUCAGAUGUGGAUGAATT), EGFL7-Homo-400 antisense (UUCAUCCACAUCUGACUGGTT), EGFL7-Homo-579 sense (GUGCAAUGAAGGAAGAAGAAG UTT), and EGFL7-Homo-579 antisense (ACUUCUUCC UUCAUUGCACTT). The Notch splitting selective inhibitor YO-01027/DBZ (Adooq® Bioscience, Nanjing, China; A11174), a dipeptide γ-secretase inhibitor, was used at 0.5 μM to inhibit Notch signaling based on previous studies [28].

Cell Proliferation Assay

To investigate the effect of rhEGFL7 on the proliferation of hBMSCs, cells were inoculated in 96-well plates at a density of 2000/well, and each of the six concentrations was repeated five times. Phosphate-buffered saline (PBS) was added to the outermost ring of the plate. After the cells were cultured for 24, 48, and 72 h at 0–1000 ng/ml of EGFL7, the medium was replaced with low-sugar Dulbecco's modified Eagle's medium (L-DMEM) containing 10 µl of Cell Counting Kit-8 Reagent (CCK-8; Boster Bio, Pleasanton, CA, USA; AR1160) and incubated at 37 °C for 0.5 h. Absorbance was measured at 450 nm using a SpectraMax® ABS (Molecular Devices, San Jose, CA, USA; ABS00369).

Osteogenic Differentiation Induction

hBMSC osteogenic differentiation induction medium was prepared as follows: 250 ml of L-DEME with 10% fetal bovine serum, 100 U/ml of penicillin and streptomycin, 10 mM β-phosphoglycerol (Sigma-Aldrich, St. Louis, MO, USA), 0.2 mM vitamin C (Sigma-Aldrich), and 100 nM dexamethasone (Sigma-Aldrich). Osteogenic induction medium was changed every 3 days.

Alkaline Phosphatase (ALP) Staining and Activity Assay

To assess early mineralization, we performed ALP staining (Beyotime, Jiangsu, China; C3206) of cells at 3 days of osteogenic induction. According to the manufacturer's instructions, cells were washed three times with PBS, fixed with 4% paraformaldehyde for 15 min, and washed with double-distilled water (ddH_2O) three times. The BCIP/NBT working solution was added and the cells were incubated at room temperature for 10 min in the dark (Beyotime; P0321S). Cells were lysed with RIPA buffer and the supernatant and 50 µl of para-nitrophenyl phosphate (pNPP) was added to a 96-well plate. Testing buffer was added to a final volume of 100 µl. An ALP standard curve was prepared with 0.5 mM p-nitrophenol. The reaction was incubated at 37°C for 10 min and stopped with the addition of 100 µl of reaction termination solution per well. Absorbance was measured at 405 nm (SpectraMax® ABS, Molecular Devices; ABS00369).

Alizarin Red S (ARS) Staining

To assess late mineralization, we performed ARS staining of cells from 12 days of osteogenic induction. Adherent cells were fixed in 4% paraformaldehyde at room temperature for 15 min, washed three times with ddH_2O, treated with ARS staining solution for 2 min, and finally washed with ddH_2O. Quantitative staining was performed by incubating the cells with 10% cetylpyridinium chloride (Sigma-Aldrich). The absorbance was measured at 560 nm (SpectraMax® ABS, Molecular Devices).

siRNA Transfection

After the hBMSCs had grown to 50% density in 6-well plates, the cells were incubated with Opti-MEM™ (Gibco, Waltham, MA, USA; 11,058,021) at 37 °C for 20 min followed by Opti-MEM™ containing 2.5 µl/ml of Lipo6000™ transfection reagent (Beyotime; C0526) and 2.5 µl/ml of siRNA for 4 h. Following transfection, Opti-MEM™ was replaced with adult BMSC complete medium (Cyagen Biosciences; HUXMA-90011).

Overexpressing Lentivirus Transfection

When hBMSCs were confluent to 50% density, the medium containing MOI 50 lentivirus and 5ug/ml Polybrene was replaced and transfected for 24 h. After 3 days, the cells were screened with puromycin and passaged for subsequent experiments.

RNA extraction and qRT-PCR

Cells were seeded in 6-well plates and induced to undergo osteogenic differentiation. Then, 600 µl of TRIzol was added to each well and the cells were lysed on ice for 5 min and aspirated into 1.5 ml microfuge tubes. Then, 200 µl of chloroform was added and the samples were shaken for 5 min and centrifuged at 4 °C and 12,000 rpm for 15 min. Next, 400 µl of the supernatant following centrifugation was transferred to a new microfuge tube, and 500 µl of isopropanol was added. The samples were shaken and centrifuged at 4 °C and 12,000 rpm for 10 min. The supernatant was discarded, 1 ml of 75% ethanol was added, and the samples were centrifuged at 4 °C and 7,500 g for 5 min. The supernatant was discarded and the pellets were dried for 5 min. The RNA concentration was measured by adding 20 µl of DEPC water. PCR was performed with an ABI7500 (Thermo Fisher, Waltham, MA, USA) with the following conditions: 95 °C for 30 s and 95 °C for 5 s for 40 cycles and 60 °C for 30 s. The $2^{-\Delta\Delta Ct}$ method was used to assess relative target gene expression [29].

Protein Extraction and Western Blotting

For 6-well plates, cells were lysed with RIPA buffer (Boster Bio; AR0105) containing protease inhibitor (Boster Bio; AR1182) and phosphatase inhibitor (Boster Bio; AR1183) on ice for 30 min and centrifuged at 4 °C and 12,000 rpm for 10 min. Then, 120 µl of supernatant was added to

30 µl of denaturing 5 × SDS-PAGE protein loading buffer (Boster Bio; AR1112) and boiled at 95 °C for 5 min. Equal amounts of protein were loaded on a 10% SDS-PAGE gel (Fudebio, Hangzhou, China; FD341) for electrophoresis (Bio-Rad, Hercules, CA, USA), which was subsequently transferred to a PVDF membrane (Millipore, Billerica, MA, USA; IPVH00010), blocked with 5% nonfat milk for 1 h, washed three times with Tris-buffered saline with Tween-20 (TBST), and incubated with the following primary antibodies overnight: anti-GAPDH (1:5000, Beyotime; AF1186), anti-RUNX2 (1:1000, Cell Signaling Technology, Danvers, MA, USA; #12,556), anti-Sp7/Osterix (1:1000, Abcam, Cambridge, UK; ab209484), anti-COL1A1 (1:1000, Cell Signaling Technology; #72,026), anti-Notch1 (1:1000, Beyotime; AF5249), anti-cleaved Notch1 (1:1000, Cell Signaling Technology; #4147), and anti-Hes1 (1:1000, Cell Signaling Technology; #11,988). The next day, the membranes were washed three times with TBST, incubated with the corresponding secondary antibody (Boster Bio; BA1054) for 1 h at room temperature, washed three times with TBST, and exposed with Chemiluminescent HRP Substrate (Millipore; WBKLS0500). Optical density analysis was performed using ImageJ software (National Institutes of Health, Bethesda, MD, USA). The density of each target strip was normalized to the upper sample control (GAPDH) and expressed as a percentage increase or decrease. Results are the mean ± standard deviation (SD) of three independent experiments.

Immunofluorescence

Cells were cultured in 12- or 24-well plates and incubated for a specific time. Then, the cells were incubated with 4% paraformaldehyde (Beyotime; P0099) for 15 min, 0.1% Triton for 30 min, and the corresponding primary antibody overnight. The next day, the cells were washed three times with PBS, incubated with secondary antibodies (Boster Bio; BA1127) for 1 h at room temperature and DAPI (Beyotime; C1002) for 5 min, and finally placed under an inverted fluorescence microscope (Leica, Wetzlar, Germany) for observation. Photos were taken at the same magnification, exposure time, and contrast.

In vivo *Evaluation*

C57BL/6 mice were purchased from Viton Lever. All animal experiments included in this study were approved by the Animal Ethics Committee of the Second Hospital of Zhejiang University School of Medicine (approval number: 2021–141, 2022–066). All animal experimental operations were performed in accordance with the Regulations for the Administration of Laboratory Animals in China and the Implementing Rules for the Administration of Medical Laboratory Animals.

Fifteen male C57BL/6 mice (10 weeks, ~ 25 g) were divided into three groups randomly: control group (no drug administration), PBS group (local injection of PBS every 3 days), and EGFL7 group (local injection of 15 µg of recombinant EGFL7 protein every 3 days). In the EGFL7 experimental group, rmEGFL7 was injected in the surgical area below the muscle, on the periosteal surface. Four experienced orthopedic surgeons performed the surgical procedures. The femoral defect model was established based on a previous study [30]. For anesthesia, mice were administered a 30 mg/kg intraperitoneal injection of 0.3% pentobarbital (Sigma-Aldrich). The right leg of the mouse was sterilized with alcohol and a sterile hole towel was laid over it. A longitudinal incision was made along the lateral side of the femur. The soft tissue was bluntly dissected, the lateral femoral was exposed, and a 1.5 mm diameter hole was drilled at 5 mm above the condyle with a 20 ml syringe needle and drilled through one side of the bone cortex. The wound was washed with saline and the skin was sutured. The same leg was used in each group. When the femoral defect was established 4 weeks later, the mice were euthanized and the right femur was removed for micro-computed tomography (CT) imaging and tissue embedding.

Micro-CT Imaging

We scanned femurs isolated from mice with MILabs U-CT (Utrecht, The Netherlands; serial number 80490). Three-dimensional reconstruction analysis was performed using Imalytics Preclinical software (version 2.1.8.9) [31]. Morphometric analysis began with the first slice of the bone defect site in the distal femur and extended proximally with the last slice of the defect site. We selected a region of interest with this standard and used the threshold tool to automatically frame the bone tissue for subsequent analysis. Bone volume fraction (BV/TV), trabecular thickness (Tb.Th), trabecular separation (Tb.Sp), specific bone surface (BS/BV), and bone mineral density (BMD) parameters were used to assess bone healing at the defect site.

Bone Histology and Histomorphometric Analysis

The femur (after CT imaging) was oscillated in decalcification solution for 30 days followed by dehydration and paraffin embedding. Then, 4 mm sagittal sections were prepared for histological analysis. For morphological analysis, sections were stained with modified hematoxylin and eosin (H&E) to visualize the bone cortex and Masson staining to visualize collagen fibers. Images were stitched together using an Olympus optical microscope (Tokyo, Japan; 163–0914). The bone cortical thickness at the defect site was measured using ImageJ software and normalized with the contralateral bone cortex.

Statistical Analysis

Image semi-quantitative analysis was performed using ImageJ software. Statistical analysis was performed using GraphPad Prism 9.0 software (San Diego, CA, USA). At least three independent replicates were performed for each experiment and data are expressed as means ± SD. Two-tailed t-tests were used for two-group analysis and a one-way analysis of variance was used for data beyond two-group analysis with Bonferroni post-hoc test for significance testing. $P < 0.05$ was considered statistically significant.

Results

EGFL7 Expression Levels in Fracture Microenvironments Increased With Age

Previous studies have shown that changes in bone marrow ecotone signaling distort mesenchymal genealogical differentiation. We download publicly available bulk RNA-sequencing gene expression profiling of skeletal stem cells (mSSCs) from fracture callus tissue of mice at different ages in the GSE166441 dataset [19]. A total of 1296 DEGs were identified, of which 553 were upregulated and 743 downregulated after differential expression analysis. Expression of EGFL7 increased 1.948-fold at the fracture site in 24-month-old mice compared with 2-month-old mice (Fig. 1A). Thirty-seven genes were considered to exhibit PPIs with EGFL7 in the STRING database (criteria confidence, $n = 0.4$) (Fig. 1D). GO enrichment analysis [25] was performed and *Notch binding* was strongly enriched in these EGFL7-related genes (Fig. 1C). The top 20 genes with the strongest interaction with EGFL7 identified by GeneMANIA were functionally enriched in the *Notch signaling pathway* and *mesenchymal stem cell differentiation* (Fig. 1B). WikiPathways in Enrichr [26, 27] was used for pathway analysis; intriguingly, *Notch signaling pathway* and *osteoblast differentiation* were ranked top ten in the enrichment results (Fig. 1E), suggesting that the EGFL7 gene plays an important role in osteogenesis. To verify this hypothesis, we first investigated the endogenous expression of EGFL7 in hBMSCs during osteogenesis. Interestingly, the expression of EGFL7 increased with the osteogenic markers RUNX2 and COLA1 (Fig. 1F).

Knockdown of EGFL7 Inhibits the Osteogenic Differentiation of hBMSCs While Overexpression Promotes

To understand the contribution of EGFL7 to stereotyping and maintenance of the osteoblast lineage, we knocked down EGFL7 in hBMSCs. EGFL7 mRNA and protein expression was significantly reduced in hBMSCs transfected with EGFL7-RNAi compared to negative control RNAi (Fig. 2A). Compared to si187 and si400, si579 had a higher knockdown efficiency at the mRNA and protein levels and was used in subsequent experiments (Fig. 2A). Immunofluorescence verified the decrease in EGFL7 expression (Fig. 2E). Knockdown of EGFL7 significantly suppressed the mRNA expression of the osteogenesis-related genes RUNX2, SP7, OCN, ALP, OPN, and COL1A1 at 3 days of osteoblast induction (Fig. 2B). Protein expression of the osteogenic genes RUNX2 and SP7 showed a decrease after EGFL7 knockdown at 3 days of osteoblast induction (Fig. 2C). EGFL7 knockdown also resulted in a decrease in ALP activity (Fig. 2F). These observations suggest that EGFL7 is required for normal osteogenic differentiation, and the knockdown of EGFL7 inhibits the osteogenesis of hBMSCs. To further validate the effect of EGFL7 on osteogenesis, we transfected hBMSCs with overexpressing lentivirus and we found that the expression of osteogenic markers (RUNX2, COL1A1) was enhanced in the EGFL7 overexpressing cells (Fig. 2D).

Recombinant EGFL7 Promotes the Osteogenic Differentiation of hBMSCs

To determine whether recombinant EGFL7 has a facilitative effect on the osteogenesis of hBMSCs, we added exogenous recombinant human EGFL7 to the osteogenic induction medium. First, 0–1000 ng/ml of rhEGFL7 had no significant effect on the proliferation of hBMSCs as shown by a CCK-8 assay (Supplementary Fig. 1A). Second, rhEGFL7 promoted osteogenesis-related gene protein (RUNX2, SP7, and COL1A1) expression at 3 days of osteoblast induction (Fig. 3A). However, the boosting effect at 0.1 ng/ml was not significantly different from that at 0 ng/ml and diminished when the concentration reached 1000 ng/ml (Fig. 3A). We then explored the effect at 5 days of osteogenic induction at 0–100 ng/ml rhEGFL7. Again, the expression of the osteogenesis-related genes RUNX2, SP7, and COL1A1 increased with increased rhEGFL7 (Fig. 3A). Immunofluorescence showed that the fluorescence intensity of RUNX2 in the nucleus and COL1A1 in the cytoplasm increased with increasing rhEGFL7 at 5 days of osteoblast induction (Fig. 3B). At 12 days after osteogenic induction, osteogenic induction medium containing rhEGFL7 protein increased calcium nodule activity (Fig. 3C). These findings suggest that EGFL7 is a positive regulator of the osteoblast phenotype and maturation in hBMSCs.

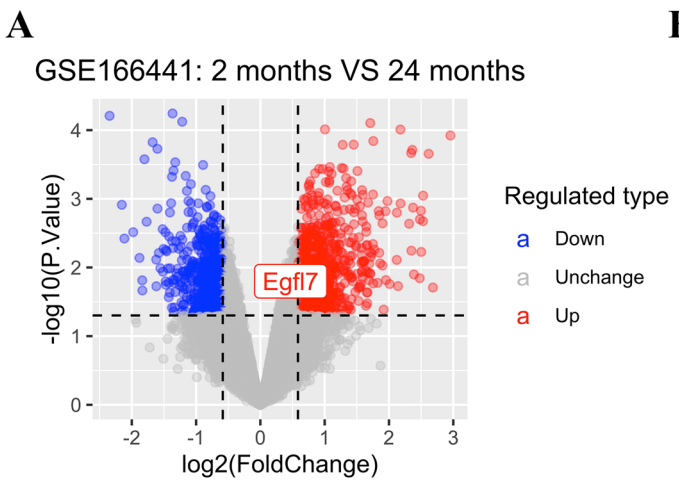
A
GSE166441: 2 months VS 24 months
-log10(P.Value)
log2(FoldChange)
Egfl7
Regulated type
Down
Unchange
Up

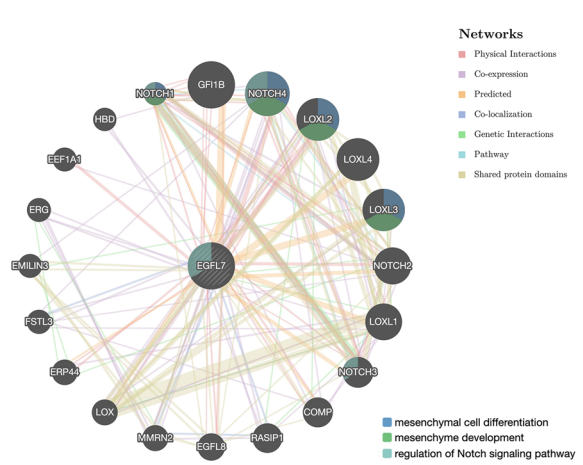
B
Networks
Physical Interactions
Co-expression
Predicted
Co-localization
Genetic Interactions
Pathway
Shared protein domains
EGFL7
mesenchymal cell differentiation
mesenchyme development
regulation of Notch signaling pathway

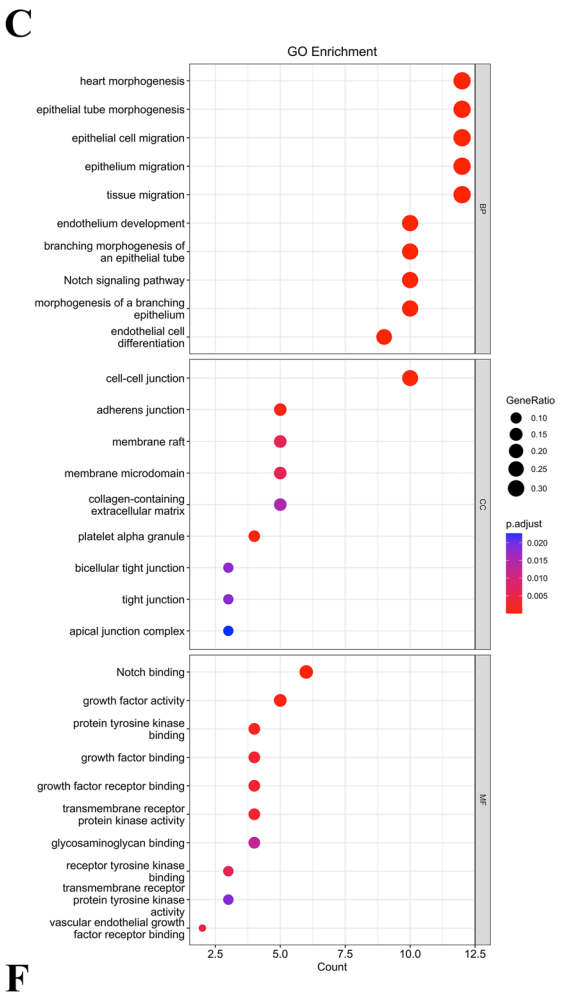
C
GO Enrichment
heart morphogenesis
epithelial tube morphogenesis
epithelial cell migration
epithelium migration
tissue migration
endothelium development
branching morphogenesis of an epithelial tube
Notch signaling pathway
morphogenesis of a branching epithelium
endothelial cell differentiation
cell-cell junction
adherens junction
membrane raft
membrane microdomain
collagen-containing extracellular matrix
platelet alpha granule
bicellular tight junction
tight junction
apical junction complex
Notch binding
growth factor activity
protein tyrosine kinase binding
growth factor binding
growth factor receptor binding
transmembrane receptor protein kinase activity
glycosaminoglycan binding
receptor tyrosine kinase binding
transmembrane receptor protein tyrosine kinase activity
vascular endothelial growth factor receptor binding
BP
CC
MF
GeneRatio
p.adjust
Count

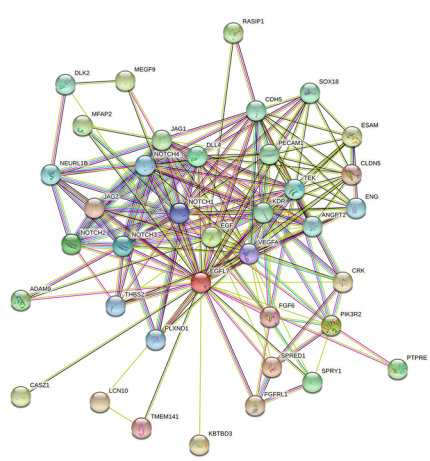
D

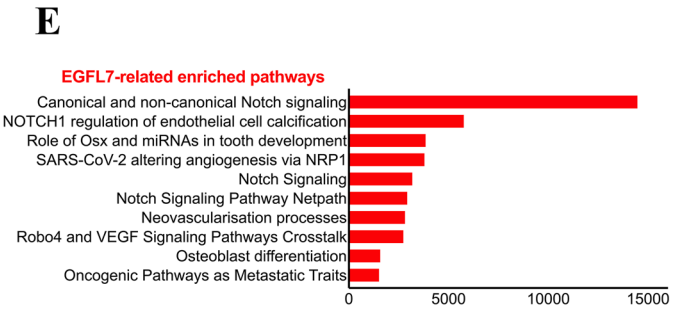
E
EGFL7-related enriched pathways
Canonical and non-canonical Notch signaling
NOTCH1 regulation of endothelial cell calcification
Role of Osx and miRNAs in tooth development
SARS-CoV-2 altering angiogenesis via NRP1
Notch Signaling
Notch Signaling Pathway Netpath
Neovascularisation processes
Robo4 and VEGF Signaling Pathways Crosstalk
Osteoblast differentiation
Oncogenic Pathways as Metastatic Traits
0
5000
10000
15000

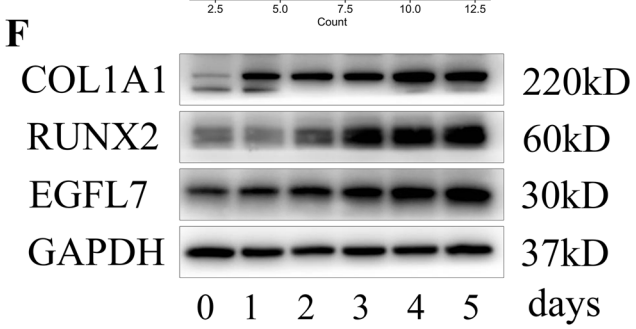
F
COL1A1
220kD
RUNX2
60kD
EGFL7
30kD
GAPDH
37kD
0 1 2 3 4 5 days

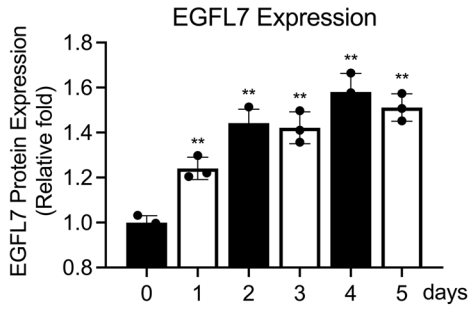
EGFL7 Expression
EGFL7 Protein Expression (Relative fold)
0 1 2 3 4 5 days

◂**Fig. 1** EGFL7 expression is upregulated during osteogenic differentiation of hBMSCs. **(A)** Volcano map of differentially expressed genes in the 24 months mice fracture site compared with 2 months (GSE166441). **(B)** TOP20 genes have protein protein interaction with EGFL7 (GeneMANIA). **(C-E)** GO analysis bubble maps and KEGG analysis (WikiPathways) of 38 EGFL7-related genes (STRING). **(F)** Western blot and quantitation of EGFL7 protein expression during osteogenic differentiation of hBMSCs for 5 days. Expressions were normalized to GAPDH. Data are shown as means ± SD of three independent experiments. $*P<0.05$, $**P<0.01$ compared with the control group

Recombinant EGFL7 Promotes Osteogenesis of hBMSCs Via The Downregulation of Notch1 Signaling

To explore the molecular mechanisms by which EGFL7 regulates osteogenic differentiation, we examined the phosphorylation status of several components involved in the osteogenesis of hBMSCs. The activated form of β-catenin and STAT3 did not change significantly compared with their total protein under rhEGFL7 stimulation (Fig. 4C). Notch1 signaling pathway is progressively downregulated with osteogenic differentiation (Fig. 4A). Further we found that inhibition of Notch pathway using AMD3100, 0.5uM promotes osteogenic differentiation (Fig. 4B). EGFL7 is considered an extracellular antagonist of classical Notch signaling [6], which prompted us to explore whether Notch signaling is inhibited by EGFL7 during osteogenic differentiation. Interestingly, expression of the intracellular domain of Notch1 (NICD) was significantly reduced in cells cultured with rhEGFL7 (Fig. 4C). Moreover, expression of Hes1, a downstream gene of the Notch pathway, decreased with increasing rhEGFL7 (Fig. 4C). In addition, we found that the ratio of phosphorylated AKT to total AKT, phosphorylated ERK to total ERK increased with increases in the rhEGFL7 concentration, indicating that the AKT and ERK pathway was also activated during the osteogenic differentiation of hBMSCs in response to rhEGFL7 stimulation (Fig. 4C). We further explored the changes of mRNAs downstream of Notch signaling pathway under rEGFL7 100 ng/ml treatment. Interestingly, Notch1 ~ 4 as well as Hes1,Hes2/4,Hey1 mRNAs were down-regulated under rEGFL7 treatment (Fig. 4D).

A Notch Signaling Pathway Inhibitor Rescued the Osteogenic-Inhibitory Effect of the EGFL7 Knockdown During hBMSC Osteogenesis

To confirm that Notch1-NICD-Hes1 signaling is important in the mechanism by which EGFL7 promotes hBMSC osteogenesis, we examined the effect of the Notch pathway inhibitor YO-01027/DBZ on the osteo-promoting effect of EGFL7. Following transfection with siNC and si579, expression of the osteogenesis-related genes RUNX2 and SP7 was decreased after EGFL7 knockdown at 3 days of osteoblast induction (Fig. 5A). Following treatment with 500 nM YO-01027 to inhibit Notch cleavage, the EGFL7 knockdown-induced decrease in RUNX2 and SP7 expression at day 3 was almost completely lost (Fig. 5A). Cleaved Notch1 and Hes1, two important markers of classical Notch signaling activation, was increased after EGFL7 knockdown at 3 days of osteoblast induction, indicating activation of classical Notch signaling (Fig. 5A). Total Notch1 protein expression was also increased in EGFL7 knockdown hBMSCs at 3 days of osteoblast induction and then decreased (Fig. 5A). The decreased RUNX2 and COL1A1 fluorescence intensity observed at day 3 of osteoblast induction after EGFL7 knockdown was rescued by YO-01027 treatment (Fig. 5B). Similarly, the downregulated ALP activity was restored by YO-01027 (Fig. 5C). These results suggest that the EGFL7 knockdown-induced inhibition of hBMSC osteogenesis was rescued by Notch signaling inhibition, indicating that EGFL7 promotes osteogenesis of hBMSCs via the downregulation of Notch1/Hes1 signaling.

Recombinant EGFL7 Accelerates Bone Healing in a Mouse Femur Defect Model

To examine the effect of EGFL7 on bone healing in vivo, we generated a 1.5 mm diameter critical size femoral defect model in the right femur of male C57BL/6 mice. In the control and PBS groups, the bone defects were clear; cortical bone in these areas was not continuous after 4 weeks (Fig. 6A). In the EGFL7 group, micro-CT images showed newly formed cortical bone and a significant increase in thickness in the bone defect area (Fig. 6A). Quantitative analysis showed that the BV/TV, Tb.Th, and BMD were higher and the Tb.Sp was lower in the EGFL7 group compared with the control and PBS groups (Fig. 6A). H&E and Masson staining showed improved healing of femoral defects in the EGFL7 group compared with the other two groups (Fig. 6B). Woven bone was observed at the site of the femoral defect and bone scab remodeling was almost complete in the EGFL7 group. There was significant bone cortical thinning and discontinuity at the femoral site in the control and PBS groups (Fig. 6B).

SP7 acts downstream of Runx2/Cbfa1 and is required for the differentiation of Runx2/Cbfa1-expressing preosteoblasts into mature osteoblasts [32]. Immunofluorescence analysis showed higher $SP7^{+}$ osteoblast numbers in the EGFL7 group compared with the control and PBS groups (Figs. 6C). Micro-CT images, quantitative measurements, histological staining, and histological immunofluorescence of the distal femur demonstrated that the EGFL7 group showed enhanced bone healing compared to the control and PBS groups. Overall, our study demonstrates a new function for EGFL7 in the promotion of hBMSC osteogenesis in vitro and in vivo.

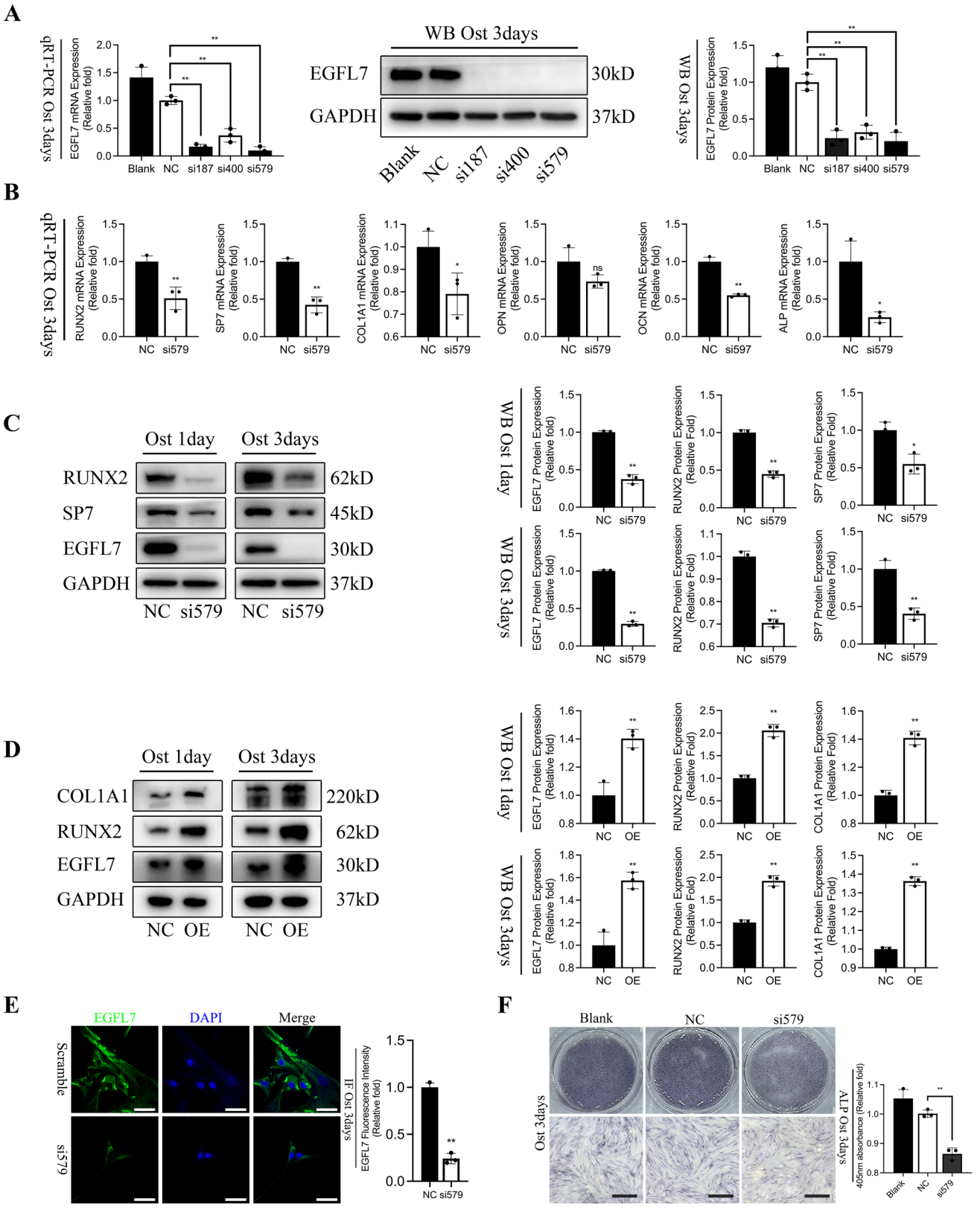
A
qRT-PCR Ost 3days
EGFL7 mRNA Expression (Relative fold)
Blank NC si187 si400 si579
WB Ost 3days
EGFL7
GAPDH
30kD
37kD
Blank NC si187 si400 si579
WB Ost 3days
EGFL7 Protein Expression (Relative fold)
Blank NC si187 si400 si579
B
qRT-PCR Ost 3days
RUNX2 mRNA Expression (Relative fold)
SP7 mRNA Expression (Relative fold)
COL1A1 mRNA Expression (Relative fold)
OPN mRNA Expression (Relative fold)
OCN mRNA Expression (Relative fold)
ALP mRNA Expression (Relative fold)
NC si579
NC si597
C
Ost 1day
Ost 3days
RUNX2
SP7
EGFL7
GAPDH
62kD
45kD
30kD
37kD
NC si579 NC si579
WB Ost 1day
WB Ost 3days
EGFL7 Protein Expression (Relative fold)
RUNX2 Protein Expression (Relative Fold)
SP7 Protein Expression (Relative Fold)
NC si579
D
Ost 1day
Ost 3days
COL1A1
RUNX2
EGFL7
GAPDH
220kD
62kD
30kD
37kD
NC OE NC OE
WB Ost 1day
WB Ost 3days
EGFL7 Protein Expression (Relative fold)
RUNX2 Protein Expression (Relative Fold)
COL1A1 Protein Expression (Relative Fold)
NC OE
E
EGFL7
DAPI
Merge
Scramble
si579
IF Ost 3days
EGFL7 Fluorescence Intensity (Relative fold)
NC si579
F
Blank
NC
si579
Ost 3days
ALP Ost 3days
405nm absorbance (Relative fold)
Blank NC si579

◂**Fig. 2** Knockdown of EGFL7 inhibits osteogenic differentiation of hBMSCs while overexpression promotes**. (A-**) Relative EGFL7 mRNA and protein expression at 3 days after EGFL7 knockdown with 3 siRNAs. **(B)** Relative mRNA expression of osteogenic-related genes (RUNX2, SP7, OCN, ALP, OPN, COL1A1) at 3 days of osteogenic induction after EGFL7 knockdown with si579. **(C-D)** Relative protein expression and quantitation of EGFL7, RUNX2, SP7 at 1, 3 days of osteogenic induction after EGFL7 knockdown and overexpression. **(E)** Represent immunofluorescence images and quantitation of EGFL7 protein at 3 days after EGFL7 knockdown with si579. **(F)** Alkaline phosphatase staining and quantitation at 3 days of osteogenic induction after EGFL7 knockdown with si579. Scale bars, 500 um. All data are shown as means ± SD of three independent experiments. $*P<0.05$, $**P<0.01$ compared with the control group. Scale bars, 50 um

Discussion

To the best of our knowledge, this is the first study to investigate the effects of EGFL7 on the osteogenic differentiation of hBMSCs. We showed that expression of EGFL7 was increased during the osteogenesis of hBMSCs. Knockdown of EGFL7 in hBMSCs inhibited osteogenesis-related gene expression at both the mRNA and protein levels while overexpression promotes it. rhEGFL7 neither promoted nor inhibited the proliferation of hBMSCs. Osteogenic-specific gene expression levels were increased in a dose-dependent manner following treatment with rhEGFL7. ARS staining

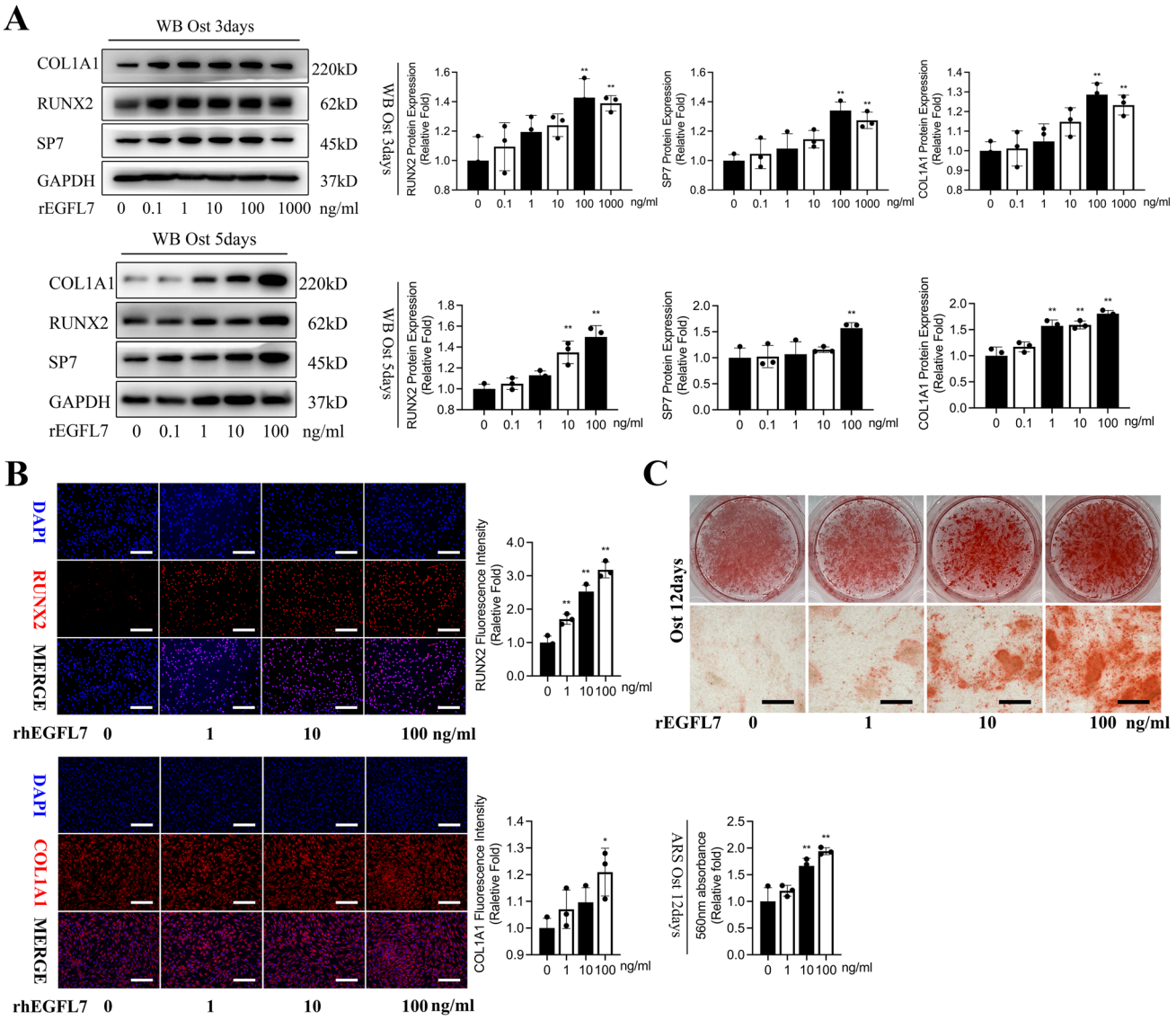

Fig. 3 Recombined EGFL7 protein promotes osteogenic differentiation of hBMSCs. **(A)** Relative protein expression and quantitation of osteo-specific genes (RUNX2, SP7 and COL1A1) at 3 days of 0 ~ 1000 ng/ml and 5 days of 0 ~ 100 ng/ml EGFL7 treatment. All data are shown as means ± SD of three independent experiments. $*P<0.05$, $**P<0.01$ compared with the control group. **(B)** Immunofluorescence and quantification of RUNX2, COL1A1 after 5 days of 0 ~ 100 ng/ml rhEGFL7 treatment and osteogenic induction of hBMSCs. Scale bars, 100 um. **(C)** Alizarin red staining and quantification at 12 days of 100 ng/ml EGFL7 treatment and osteogenic induction. Scale bars, 500 um. All data are shown as means ± SD of three independent experiments. $*P<0.05$, $**P<0.01$ compared with the control group

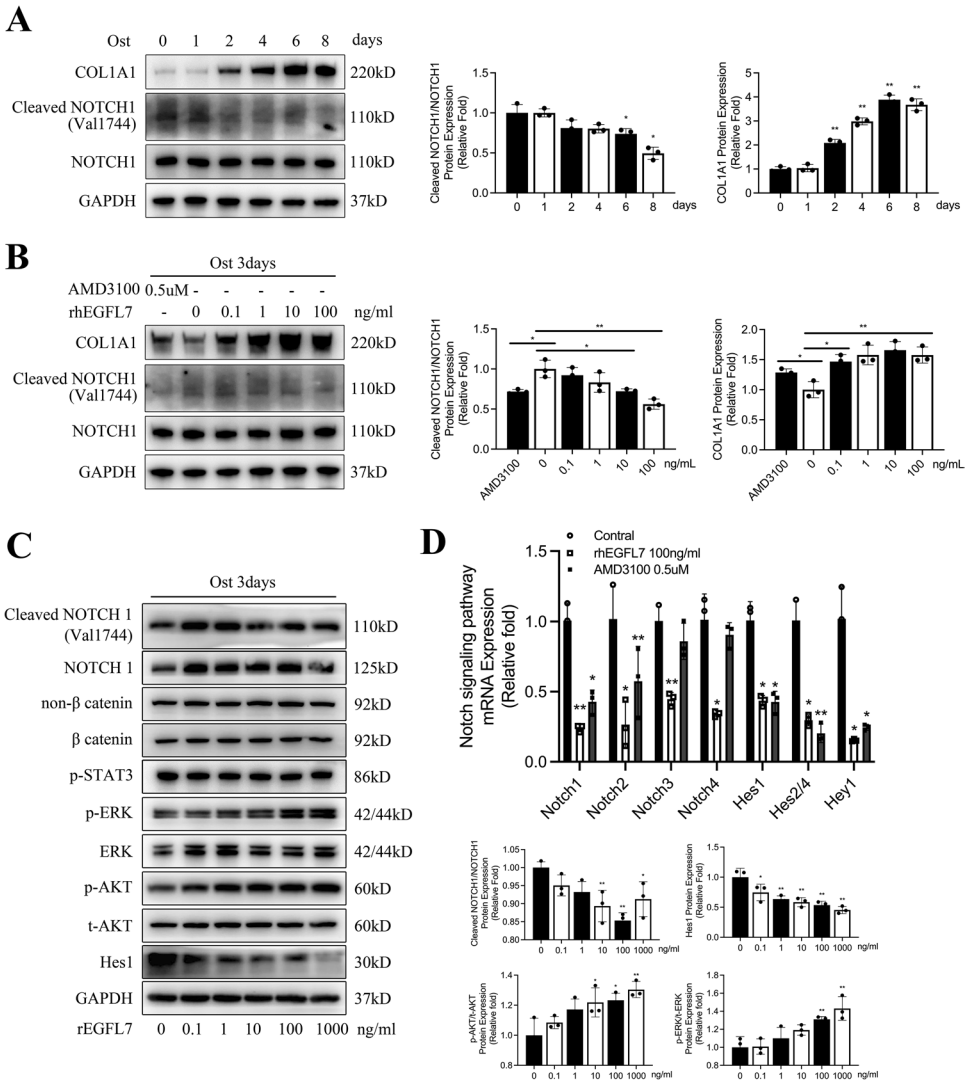

Fig. 4 Recombined EGFL7 protein promote osteogenic differentiation of hBMSCs partly via downregulating Notch1 signaling pathway. **(A)** WB and semi-quantitative maps of changes in NOTCH1 signaling pathway and COL1A1 during endogenous osteogenic differentiation from 0 to 8 days. **(B)** WB and semi-quantitative maps of the effects of AMD3100 0.5uM and rEGFL7 0-100 ng/ml treatments on osteogenic differentiation and Notch1 signaling pathway in hBMSCs. **(C)** Western blot comparison of several signaling pathway activation profiles at 3 days of 0 ~ 1000 ng/ml EGFL7 treatment and osteogenic induction. The quantitation of active ratio responds to 0 ~ 1000 ng/ml rhEGFL7 treatment and osteogenic induction at 3 days. **(D)** Changes in mRNA of genes downstream of Notch signaling pathway in hBMSCs under rhEGFL7 100 ng/ml treatment. All data are shown as means ± SD of three independent experiments. $^{*}P < 0.05$, $^{**}P < 0.01$ compared with the control group

showed that rhEGFL7 enhanced hBMSC mineralization in a dose-dependent manner. These results demonstrate that EGFL7 promotes osteogenic differentiation and enhances the mineralization of hBMSCs.

Epidermal growth factor-like factors (EGFLs) are proteins that contain different epidermal growth factor (EGF) homologous repeats, which are characterized by three disulfide bonds formed between cysteine residues [33, 34]. Their similar structures may share certain structural functions. Recently, EGF-repeats have been reported to be essential for osteogenesis [35]. Seven EGFL family members have been identified (EGFL2, EGFL3, EGFL5, EGFL6, EGFL7, EGFL8, and EGFL9) [36]. Among them, expression of EGFL3, EGFL5, EGFL6, and EGFL9 is higher in osteoblasts while EGFL2, EGFL7, and EGFL8 are abundantly expressed in both osteoblasts and osteoclasts [37]. EGFL7 and EGFL6 are the most studied EGFL family members; fewer than ten studies dedicated to other EGFL family members were identified. EGFL6 has shown to promote BMSC osteogenesis and H type angiogenesis [38–40], while the roles of the other members remain unclear. The pro-angiogenic effects (e.g., recruitment, proliferation, motility, migration, sprouting, and tube formation) of EGFL7 have been documented in a number of different cell lines (e.g., HUVECs [9, 15, 41–43], h-ESCs [44], SVECs [4], MEFs [45], C167 [45], and RVSMCs [45]). EGFL7 achieves these pro-angiogenic effects through the integrin $\alpha_V\beta_3$ (RGD-dependent manner) [41], Notch [46], ERK [4], STAT3 [4], CASZ1/RhoA [42], and VE-cadherin [43] pathways. Bone healing is a result of both osteogenesis and angiogenesis [47]. Our study found that EGFL7 is expressed in hBMSCs and promotes osteogenic differentiation.

EGFL7 contains an EMI structure that binds strongly to Notch receptors [6]. In the present study, rhEGFL7 downregulated Notch-specific genes (e.g., NICD and HES1) in a dose-dependent manner. EGFL7 knockdown activated Notch signaling, while the addition of a γ-secretase inhibitor (YO-01027/DBZ) rescued EGFL7 knockdown-induced

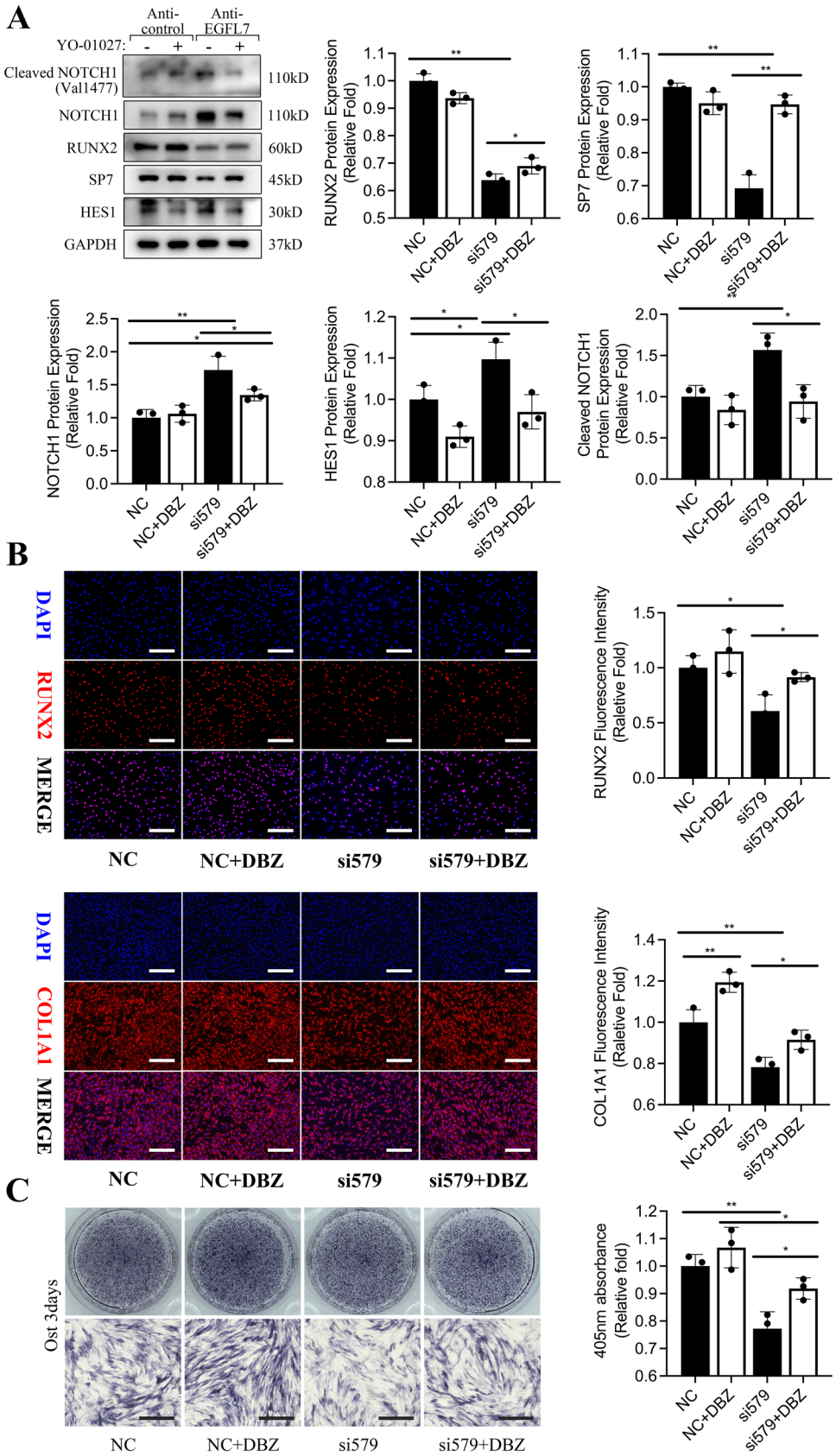

Fig. 5 Notch1 signaling pathway inhibitor rescued the osteogenesis-inhibitory effect of EGFL7 knockdown. **(A)** Western blot and quantitation comparison of Notch signaling pathway markers (Cleaved Notch1, Notch1, Hes1) and osteo-specific genes (RUNX2, SP7) at 3 days of YO-01027/DBZ(0.5uM) (Ic50 2.9 nM) treatment and osteogenic induction in EGFL7 knockdown hBMSCs. **(B)** Immunofluorescence and quantification of the osteo-specific genes (RUNX2, COL1A1) at 3 days of YO-01027 treatment and osteogenic induction in EGFL7 knockdown hBMSCs. Scale bars, 100 um. **(C)** Alkaline phosphatase staining and quantification at 3 days of YO-01027 treatment and osteogenic induction in EGFL7 knockdown hBMSCs. Scale bars, 500 um. All data are shown as means ± SD of three independent experiments. $^{*}P < 0.05$, $^{**}P < 0.01$ compared with the control group

osteogenic inhibition. Our results are consistent with the findings of several previous studies investigating the relationship between osteogenesis and Notch signaling. Overexpression of NICD inhibits osteogenic differentiation [48–51]. Hes1 and Hey1 [52], downstream genes in the Notch signaling pathway, interact with RUNX2 and repress its activity [53, 54]. Notch-Hey1/HeyL also inhibit osteogenic differentiation by repressing NFATc1 transcription [55]. Notch signaling helps maintain the number of BMSCs [53, 54]; Notch expression in immature and mature osteoblasts impairs osteoblast differentiation and leads to a reduced bone mass [56]. EGFL7 expression in the bone microenvironment reduces Notch signaling; this altered Notch signaling resulted in a shift in the differentiation pattern of BMSCs toward excess osteoblasts. Our finding that BMSCs are a source of EGFL7 in fracture hematomas suggests that stem cell-derived EGFL7 acts as an endogenous antagonist of Notch1 signaling and regulates the differentiation of hBMSCs in bone defect sites. At the same time, ERK and AKT signaling pathways were also activated in hBMSCs

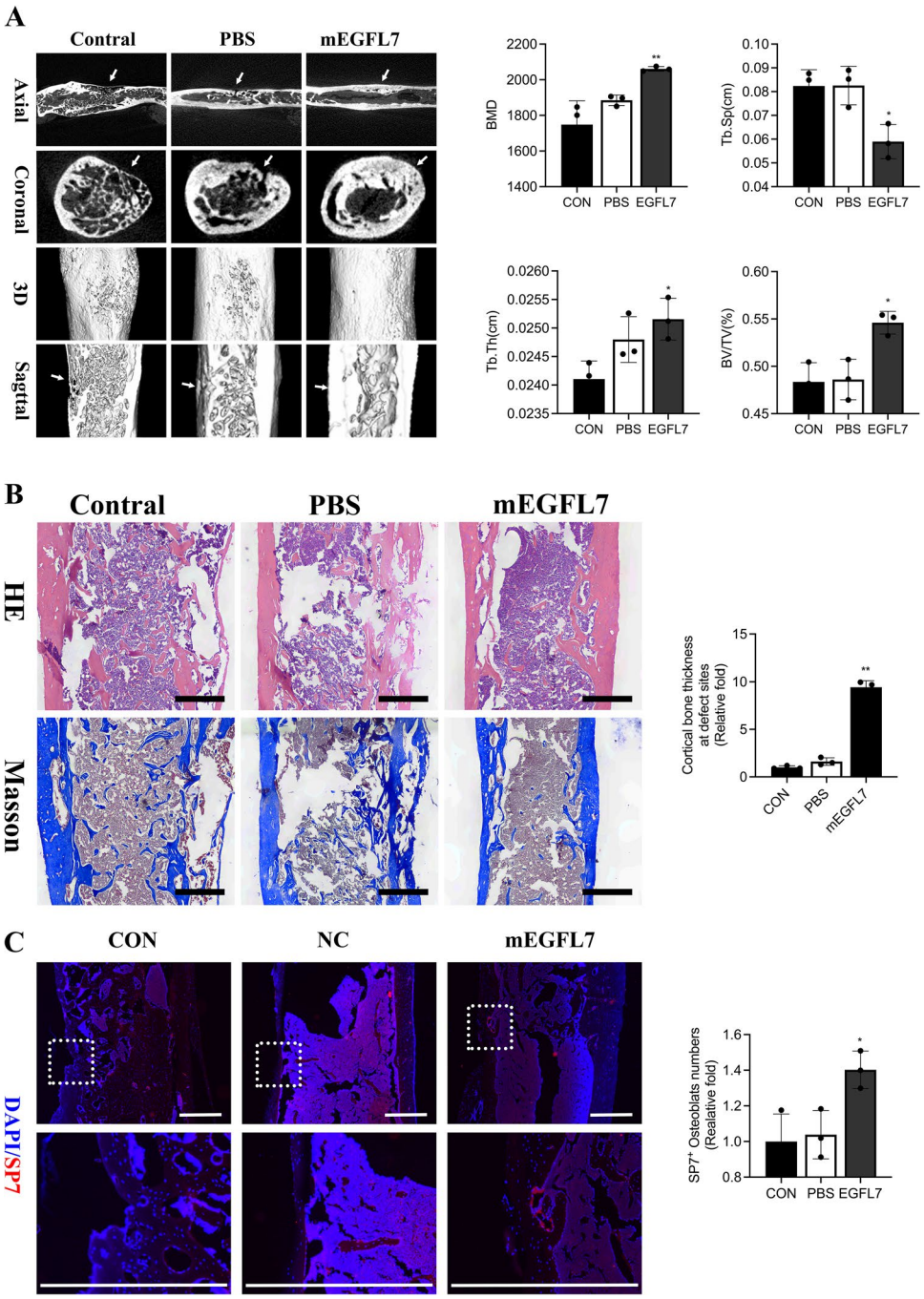

Fig. 6 Recombined EGFL7 protein promotes healing of femoral defects in mice. **(A)** Representative micro-CT images and quantitative analysis (BMD, Tb.Sp, Tb.Th,BV/TV) of femoral defect sites in 3 groups. **(B)** Representative images of HE and Masson staining and quantification of cortical bone thickness of femoral defect sites in 3 groups. **(C)** Representative images and quantification of SP7 histology immunofluorescence staining at the femoral defect sites in 3 groups. Scale bars, 500 um. All data are shown as means ± SD of three independent experiments. $^{*}P < 0.05$, $^{**}P < 0.01$ compared with the control group

under rEGFL7 treatment, while STAT3 and FAK signaling pathways were not significantly changed. rEGFL7 was previously reported to activate ERK, FAK, and STAT3 pathways [4], and we consider this to be a different mechanism of action of EGFL7 on different cells.

The femur diaphyseal defect is a classic bone healing model [30]. It disrupts one side of the cortex with moderate marrow scraping. Bone defects not involving fractures not only ensure less pain, but also make the bone healing process easier to quantify [57]. Our in vivo studies showed that rhEGFL7 increased the number of $SP7^+$ osteoblasts at bone defect sites. rhEGFL7 also accelerated lamellar bone deposition and bone cortical thickness; rhEGFL7 also enhanced the trabecular thickness, bone volume, and bone mineral density of newly formed bone and decreased trabecular separation in the cavity, demonstrating that rhEGFL7 promotes bone healing of femoral defects in vivo. A recent study by Jiake Xu et al. [58]. using single-cell sequencing showed that EGFL7 is abundantly expressed by endothelial cells, strongly suggesting a pro-angiogenic role for EGFL7. Bone healing is a process of osteogenesis and angiogenesis coupling. The dual promotion of angiogenesis [41–44] and osteogenesis by EGFL7 makes it a promising new target for the future clinical treatment of bone nonunion.

Our study has some limitations. First, our study is based on experimental results from in vitro stem cells and bone defect models and did not use transgenic mice. Second, we did not investigate changes in all signaling pathways following treatment with EGFL7. It is possible that EGFL7 regulates the osteogenic differentiation of hBMSCs via several different pathways.

In summary, we demonstrate a new function of EGFL7, and we expand the molecular mechanisms by which EGFL7 acts as a positive regulator of hBMSC osteogenic differentiation. Our study suggests a new mechanism by which the EGFL7-Notch1-NICD-Hes1 pathway reprograms hBMSCs for osteoblast identity. In the future, when faced with large bone defects, bone tumors, and infection-induced bone nonunion, treatment targeting EGFL7 could provide new directions for clinical applications.

Conclusion

EGFL7 promotes the osteogenesis of hBMSCs partly via downregulation of the Notch signaling pathway.

Abbreviations hBMSCs: Human bone marrow mesenchymal stem cells; EGFL7: Epidermal growth factor-like 7; rhEGFL7: Recombined human EGFL7 protein; rmEGFL7: Recombined mouse EGFL7 protein; mSSCs: Skeletal stem cells; qRT-PCR: Quantitative real-time PCR; WB: Western blot; IF: Immunofluorescence; siRNA: Small interfering RNA; NICD: Notch intracellular domain; ECs: Endothelial cells; ECM: Extracellular matrix; ICAM: Intercellular adhesion molecule; VCAM: Vascular cell adhesion molecule; h-ESC: Human embryonic stem cells; SVEC: Simian virus 40-transformed mouse microvascular endothelial cell line; MEF: Mouse embryonic fibroblasts; C167: Murine yolk sac endothelial cells; RVSMC: Rat vascular smooth muscle cells

Supplementary Information The online version contains supplementary material available at https://doi.org/10.1007/s12015-022-10503-z.

Authors' Contributions WZ, JB, and LL contributed equally to this article. WZ, JB, LL and YZ conducting in vitro experiments. KH, YW and ZW help with in vivo experiments. CY revised the manuscript and remade figures. DX supervised and managed this work. All authors read and approved the final manuscript.

Funding This research was supported by the Joint Funds of the Zhejiang Provincial Natural Science Foundation of China (No. LBY21H060004), the Zhejiang Provincial Natural Science Foundation of China (No. LQ21H060007), the National Natural Science Foundation of China (No. 81871759 and No. 82172189).

Data Availability The datasets GSE166441 for this study can be found in the GEO database. Please see the https://www.ncbi.nlm.nih.gov/geo/query/acc.cgi?acc=GSE166441 for more details.

Code Availability Not applicable.

Declarations

Conflicts of Interest/Competing Interests The authors declare that they have no competing interests.

Ethics Approval The animal experiments included in this study were approved by the Animal Ethics Committee of the Second Hospital of Zhejiang University School of Medicine (approval number: 2021–141, 2022–066).

Consent to Participate Not applicable.

Consent for Publication Not applicable.

References

1. Hak, D. J., et al. (2014). Delayed union and nonunions: Epidemiology, clinical issues, and financial aspects. *Injury, 45*(Suppl 2), S3-7.
2. Antonova, E., et al. (2013). Tibia shaft fractures: Costly burden of nonunions. *BMC Musculoskeletal Disorders, 14*, 42.
3. Phillips, A. M. (2005). Overview of the fracture healing cascade. *Injury, 36*(3), S5–S7.
4. Chim, S. M., et al. (2015). EGFL7 Is Expressed in Bone Microenvironment and Promotes Angiogenesis via ERK, STAT3, and Integrin Signaling Cascades. *Journal of Cellular Physiology, 230*(1), 82–94.
5. Lofgren, M., et al. (2014). Cell and matrix modulation in prenatal and postnatal equine growth cartilage, zones of Ranvier and articular cartilage. *Journal of Anatomy, 225*(5), 548–568.
6. Schmidt, M. H. H., et al. (2009). Epidermal growth factor-like domain 7 (EGFL7) modulates Notch signalling and affects neural stem cell renewal. *Nature Cell Biology, 11*(7), 873–880.

7. Soncin, F., et al. (2003). VE-statin, an endothelial repressor of smooth muscle cell migration. *EMBO Journal, 22*(21), 5700–5711.
8. Fitch, M. J., et al. (2004). Egfl7, a novel epidermal growth factor-domain gene expressed in endothelial cells. *Developmental Dynamics, 230*(2), 316–324.
9. Parker, L. H., et al. (2004). The endothelial-cell-derived secreted factor Egfl7 regulates vascular tube formation. *Nature, 428*(6984), 754–758.
10. Heissig, B., et al. (2021). The Multifaceted Roles of EGFL7 in Cancer and Drug Resistance. *Cancers, 13*(5), 1014.
11. Salama, Y., Hattori, K., & Heissig, B. (2017). The angiogenic factor Egfl7 alters thymogenesis by activating Flt3 signaling. *Biochemical and Biophysical Research Communications, 490*(2), 209–216.
12. Delfortrie, S., et al. (2011). Egfl7 promotes tumor escape from immunity by repressing endothelial cell activation. *Cancer Research, 71*(23), 7176–7186.
13. Lelievre, E., et al. (2008). VE-statin/egfl7 regulates vascular elastogenesis by interacting with lysyl oxidases. *EMBO Journal, 27*(12), 1658–1670.
14. Vallet, S. D., et al. (2020). The interactome of cancer-related lysyl oxidase and lysyl oxidase-like proteins. *Cancers (Basel), 13*(1), 71.
15. Dudvarski Stankovic, N., et al. (2018). EGFL7 enhances surface expression of integrin α5β1 to promote angiogenesis in malignant brain tumors. *EMBO Mol Med, 10*(9), e8420.
16. Wang, F. Y. F., et al. (2020). Proteomics identifies EGF-like domain multiple 7 as a potential therapeutic target for epidermal growth factor receptor-positive glioma. *Cancer Communications, 40*(10), 518–530.
17. Zhai, W., et al. (2019). A positive feed-forward loop between LncRNA-URRCC and EGFL7/P-AKT/FOXO3 signaling promotes proliferation and metastasis of clear cell renal cell carcinoma. *Mol Cancer, 18*(1), 81.
18. Bill, M., et al. (2020). EGFL7 Antagonizes NOTCH Signaling and Represents a Novel Therapeutic Target in Acute Myeloid Leukemia. *Clinical Cancer Research, 26*(3), 669–678.
19. Ambrosi, T. H., et al. (2021). Aged skeletal stem cells generate an inflammatory degenerative niche. *Nature, 597*(7875), 256–262.
20. Ritchie, M. E., et al. (2015). limma powers differential expression analyses for RNA-sequencing and microarray studies. *Nucleic Acids Research, 43*(7), e47.
21. Franceschini, A., et al. (2013). *STRING v9.1: protein-protein interaction networks, with increased coverage and integration. Nucleic Acids Research*, 41(Database issue), D808–15.
22. Franz, M., et al. (2018). GeneMANIA update 2018. *Nucleic Acids Research, 46*(W1), W60–W64.
23. Wu, T., et al. (2021). clusterProfiler 4.0: A universal enrichment tool for interpreting omics data. *Innovation (N Y)*, 2(3), 100141.
24. Yu, G., et al. (2012). clusterProfiler: an R Package for Comparing Biological Themes Among Gene Clusters. *OMICS: A Journal of Integrative Biology*, 16(5), 284–287.
25. Ashburner, M., et al. (2000). Gene ontology: Tool for the unification of biology. The Gene Ontology Consortium. *Nature Genetics, 25*(1), 25–29.
26. Chen, E. Y., et al. (2013). Enrichr: Interactive and collaborative HTML5 gene list enrichment analysis tool. *BMC Bioinformatics, 14*, 128.
27. Kuleshov, M. V., et al. (2016). Enrichr: A comprehensive gene set enrichment analysis web server 2016 update. *Nucleic Acids Research, 44*(W1), W90–W97.
28. Jin, W. J., et al. (2016). Supporting data for the effect of gamma-secretase inhibitors in osteoclast differentiation and spreading. *Data in Brief, 7*, 682–685.
29. Livak, K. J., & Schmittgen, T. D. (2001). Analysis of relative gene expression data using real-time quantitative PCR and the 2(-Delta Delta C(T)) Method. *Methods, 25*(4), 402–408.
30. Monfoulet, L., et al. (2010). Drilled hole defects in mouse femur as models of intramembranous cortical and cancellous bone regeneration. *Calcified Tissue International, 86*(1), 72–81.
31. Gremse, F., et al. (2016). Imalytics Preclinical: Interactive Analysis of Biomedical Volume Data. *Theranostics, 6*(3), 328–341.
32. Nakashima, K., et al. (2002). The novel zinc finger-containing transcription factor osterix is required for osteoblast differentiation and bone formation. *Cell, 108*(1), 17–29.
33. Taylor, J. M., Mitchell, W. M., & Cohen, S. (1972). Epidermal Growth Factor. *Journal of Biological Chemistry, 247*(18), 5928–5934.
34. Savage, C. R., Hash, J. H., & Cohen, S. (1973). Epidermal Growth Factor. *Journal of Biological Chemistry, 248*(22), 7669–7672.
35. Kahai, S., et al. (2010). Nephronectin promotes osteoblast differentiation via the epidermal growth factor-like repeats. *FEBS Letters, 584*(1), 233–238.
36. Lim, Y. S., et al. (2021). Descriptive and functional characterization of epidermal growth factor-like domain 8 in mouse cortical thymic epithelial cells by integrated analysis of gene expression signatures and networks. *Int J Mol Med, 47*(3), 4.
37. Chim, S. M., et al. (2011). EGFL6 promotes endothelial cell migration and angiogenesis through the activation of extracellular signal-regulated kinase. *Journal of Biological Chemistry, 286*(25), 22035–22046.
38. Shen, J., et al. (2021). EGFL6 regulates angiogenesis and osteogenesis in distraction osteogenesis via Wnt/beta-catenin signaling. *Stem Cell Research & Therapy, 12*(1), 415.
39. Chen, K., et al. (2021). Osteoblast-derived EGFL6 couples angiogenesis to osteogenesis during bone repair. *Theranostics, 11*(20), 9738–9751.
40. Liu, H., & Wang, X. (2022). Epidermal growth factor-like domain protein 6 recombinant protein facilitates osteogenic differentiation in adipose stem cells via bone morphogenetic protein 2/recombinant mothers against decapentaplegic homolog 4 signaling pathway. *Bioengineered, 13*(3), 6558–6566.
41. Nikolic, I., et al. (2013). EGFL7 ligates alphavbeta3 integrin to enhance vessel formation. *Blood, 121*(15), 3041–3050.
42. Charpentier, M. S., et al. (2013). CASZ1 promotes vascular assembly and morphogenesis through the direct regulation of an EGFL7/RhoA-mediated pathway. *Developmental Cell, 25*(2), 132–143.
43. Usuba, R., et al. (2019). EGFL7 regulates sprouting angiogenesis and endothelial integrity in a human blood vessel model. *Biomaterials, 197*, 305–316.
44. Richter, A., et al. (2019). EGFL7 Mediates BMP9-Induced Sprouting Angiogenesis of Endothelial Cells Derived from Human Embryonic Stem Cells. *Stem Cell Reports, 12*(6), 1250–1259.
45. Campagnolo, L., et al. (2005). EGFL7 Is a Chemoattractant for Endothelial Cells and Is Up-Regulated in Angiogenesis and Arterial Injury. *The American Journal of Pathology, 167*(1), 275–284.
46. Nichol, D., et al. (2010). Impaired angiogenesis and altered Notch signaling in mice overexpressing endothelial Egfl7. *Blood, 116*(26), 6133–6143.
47. Carano, R. A., & Filvaroff, E. H. (2003). Angiogenesis and bone repair. *Drug Discovery Today, 8*(21), 980–989.
48. Sciaudone, M., et al. (2003). Notch 1 impairs osteoblastic cell differentiation. *Endocrinology, 144*(12), 5631–5639.
49. Deregowski, V., et al. (2006). Notch 1 overexpression inhibits osteoblastogenesis by suppressing Wnt/beta-catenin but not bone morphogenetic protein signaling. *Journal of Biological Chemistry, 281*(10), 6203–6210.
50. Shindo, K., et al. (2003). Osteogenic differentiation of the mesenchymal progenitor cells, Kusa is suppressed by Notch signaling. *Experimental Cell Research, 290*(2), 370–380.

51. Zanotti, S., et al. (2008). Notch inhibits osteoblast differentiation and causes osteopenia. *Endocrinology, 149*(8), 3890–3899.
52. Zamurovic, N., et al. 2004 (Coordinated activation of notch, Wnt, and transforming growth factor-beta signaling pathways in bone morphogenic protein 2-induced osteogenesis. Notch target gene Hey1 inhibits mineralization and Runx2 transcriptional activity. *The Journal of Biological Chemistry*, 279(36), 37704–15.
53. Hilton, M. J., et al. (2008). Notch signaling maintains bone marrow mesenchymal progenitors by suppressing osteoblast differentiation. *Nature Medicine, 14*(3), 306–314.
54. Engin, F., et al. (2008). Dimorphic effects of Notch signaling in bone homeostasis. *Nature Medicine, 14*(3), 299–305.
55. Tu, X., et al. (2012). Physiological notch signaling maintains bone homeostasis via RBPjk and Hey upstream of NFATc1. *PLoS Genetics, 8*(3), e1002577.
56. Canalis, E., et al. (2013). Osteoblast lineage-specific effects of notch activation in the skeleton. *Endocrinology, 154*(2), 623–634.
57. Campbell, T. M., Wong, W. T., & Mackie, E. J. (2003). Establishment of a model of cortical bone repair in mice. *Calcified Tissue International, 73*(1), 49–55.
58. Feleke, M., et al. (2022). Single-cell RNA sequencing reveals differential expression of EGFL7 and VEGF in giant-cell tumor of bone and osteosarcoma. *Experimental Biology and Medicine (Maywood, N.J.), 247*(14), 1214–1227.